NUMERICAL-EXPERIMENTAL CORRELATION OF ROTOR FLOWFIELD IN GROUND EFFECT

Claudio Pasquali, claudio.pasquali@uniroma3.it, Roma Tre University (Italy)
Jacopo Serafini, jacopo.serafini@uniroma3.it, Roma Tre University (Italy)
Giovanni Bernardini, giovanni.bernardini@uniroma3.it, Roma Tre University (Italy)
Massimo Gennaretti, massimo.gennaretti@uniroma3.it, Roma Tre University (Italy)
Joseph Milluzzo, milluzzo@usna.edu, U.S. Naval Academy (USA)
Scott Davids, davids@usna.edu, U.S. Naval Academy (USA)

Abstract
This work presents the comparison between experimental measurements and numerical simulations concerning the flowfield generated by a helicopter rotor operating in ground effect conditions above an inclined plane. Specifically, the capability of a potential-based, three-dimensional, free-wake aerodynamic solver to simulate in-ground-effect problems is assessed in terms of loads and wake inflow field, showing a good agreement with the experimental data.

1. INTRODUCTION

Helicopter operations regularly require long-lasting hovering over inclined or moving surfaces (e.g., hillsides or ship decks). These challenging operational conditions significantly affect rotorcraft response and often require specific training and expensive flight tests to mitigate risks. In order to increase safety and to reduce pilot workload, advanced flight control systems are desirable. However, particularly for these operational conditions, a prerequisite to develop reliable flight control systems is the availability of reliable flight dynamics models which, in turns, requires the understanding of the complex fluid dynamics of the problem, and hence of wake shape evolution and corresponding wake effects in the presence of the ground.

Rotor wake modeling is clearly one the most important and challenging tasks in helicopter simulation of operations in proximity of the ground. Due to the complexity of this problem, a lot of free-wake algorithms have been implemented by the rotorcraft research community, with application of several different solution strategies, with the aim of capturing in ground effect (IGE) wake deformation.[15,11,17]

While there is a considerable amount of prior works examining the aerodynamics of rotors hovering above surfaces parallel to the rotor disk[12,14,3,16], the examination of the ground effect of inclined surfaces is still an almost unexplored problem. Nonetheless, this case has big practical interest, since it is typical of many piloting tasks, like landing on ships in rough sea or mountain rescue.

The goal of this paper is to investigate the flowfield of a hovering rotor wake in ground effect above inclined planes, as well as to compare the corresponding numerical simulations with experimental data.

Specifically, the numerical simulations are performed through a solver developed at Roma Tre University, based on a BEM approach for the solution of unsteady potential flows around lifting bodies, that is capable of dealing with bodies in arbitrary motion, in the presence of strong blade-vortex interactions[5]. It has been extensively validated and successfully applied to aerodynamic and aeroacoustic analyses of helicopter rotors.[9,1,7,4,6] These results are validated against the flowfield measurements performed at the U.S. Naval Academy. Indeed, this work is developed as part of the activities of Roma Tre University within the University of Maryland/U.S.Naval Academy Vertical Lift Research Center of Excellence.

This work is conceived as the first necessary step towards the development of a state-space dynamic inflow model useful for flight dynamics analysis and control applications in IGE conditions, based on a validated high-fidelity aerodynamic simulation tool.[8]

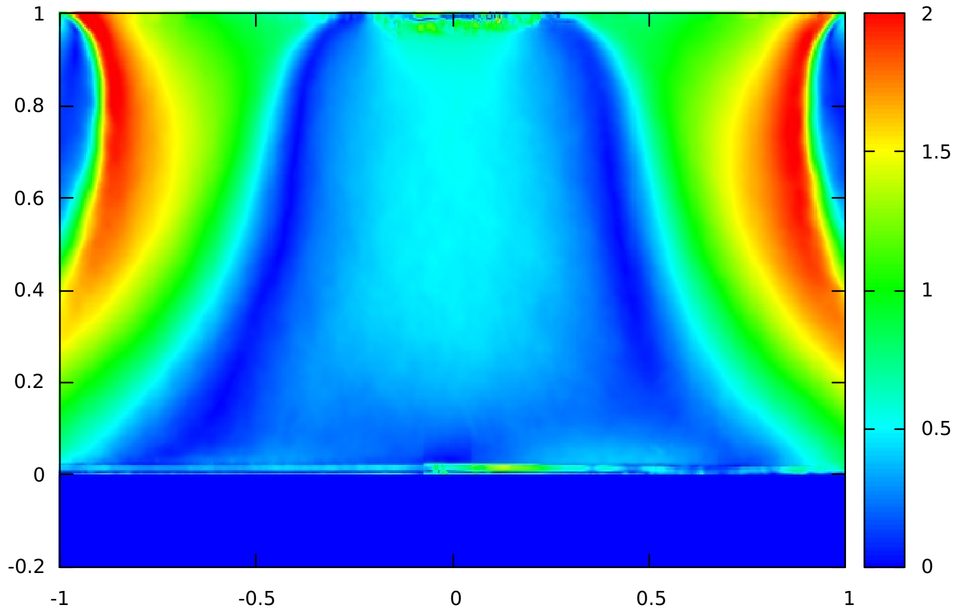

Figure 1: Experimental flow field visualization with parallel ground.

2. EXPERIMENTAL CAMPAIGN

The experimental measurement campaign has been performed at the U.S. Naval Academy experimental facilities. The resulting data include 2-C particle image velocimetry (PIV) measurements and performance measurements on a two-bladed rotor system, whose main data are summarized in Tab. 1.

The rotor has been tested out-of-ground-effect and in-ground-effect (with the rotor-ground distance equal to the rotor radius) at ground plane angles of 0 (i.e., parallel to the rotor disk), 10, 15, 20, and 30 degrees.

Radius	408 [mm]
Chord	44.8 [mm]
Airfoil	NACA 0012
Collective Pitch	6°
Angular Velocity	2100 rpm

Table 1: Two-bladed rotor main characteristics.

The hub loads were obtained using a six-axis load cell for collective pitch angles ranging from 0 to 12 degrees with 2-degree increments. Flow field measurements were performed using both a high- and a low-speed PIV system. The high-speed system comprised two 4-megapixel (1280x800) CMOS camera and the regions of interest were illuminated using a light sheet produced by a 30 mJ/pulse Nd:YLF laser. The low-speed system utilized an Nd:YAG laser capable of producing 380 mJ/pulse when operated below 10 Hz, and two 29-megapixel (6600x4400) cameras. For each measurement type the cameras were aligned adjacent with a 20% overlap in their fields of view, allowing the temporally correlated images to be stitched together. The high-speed measurements focused on a region of interest in the near field of the rotor that encompassed the entire blade. To examine the whole wakes convected from the rotor to the ground, the low-speed cameras were focused on a region encompassing the entire rotor, as well as the ground plane. Furthermore, to examine the entire structure of the rotor wake, measurements were taken at azimuthal locations of 0 to 180 degrees in 30 degree increments.

3. AERODYNAMIC SOLVER

Considering incompressible potential flows, the aerodynamic formulation applied assumes the potential field to be given by the superposition of incident and scattered potentials.

The scattered potential is determined by sources and doublets distribution over the surface of the blades and by doublets distributed over the wake portion closest to the trailing edge from which emanated (near wake).[5]

The incident potential field is associated to doublets distributed over the complementary wake region that compose the far wake. The wake surface partition is such that the far wake is the only wake portion that may come in contact with bodies (blades, ground and obstacles).

The incident potential is discontinuous across the far wake, whereas the scattered potential is discontinuous across the near wake and it is obtained by solving a boundary integral equation.[5,2]

Recalling the equivalence between surface distribution of doublets and vortices, the velocity field induced by the wake is evaluated through the Biot-Savart law applied to finite-thickness Rankine-model vortices having the shape of the panels contours. Once the potential field is known, the Bernoulli theorem yields the pressure distribution from which, in turn, blade and rotor loads can be readily evaluated.[5] The wake shape is determined as part of the solution, moving the vertices of the discretization panels in accordance with the velocity field[5] (free wake).

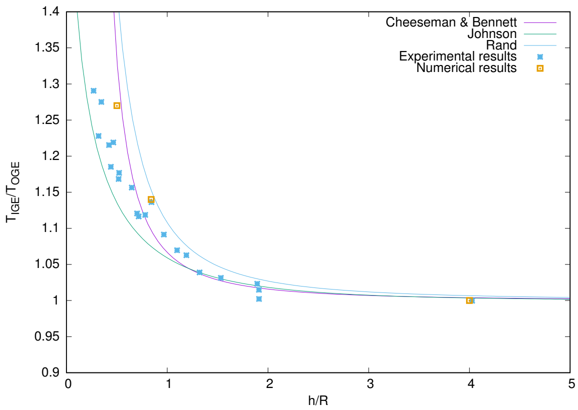

Figure 2: Ground effect on rotor thrust[10] *vs* h_g/R.

The capability of the free-wake BEM solver to predict in-ground-effect rotor aerodynamics has been partially validated against experimental data in the recent past. Indeed, two different mathematical models of the ground have been compared[10]: 1. ground considered as an impermeable boundary of the fluid domain, and hence discretized with panels of sources and doublets; 2. ground effect simulated by introduction of a specular rotor (mirror image method), thus exploiting the equivalence between impermeability of a plane and symmetrization of the aerodynamic problem with respect to that plane.

Both solvers, for ground parallel to the rotor disk and fixed collective pitch, provided the numerical prediction of the ratios of IGE and out-of-ground-effect (OGE) thrust for different values of the rotor-ground distance shown in Fig. 2. In this picture they are also compared with experimental data and three approximated analytical prediction formulas proposed in the literature.[10] Past investigation has also demonstrated the capability of the BEM solver to capture the influence of ground on the position of the near wake tip vortices.[10]

In this work, BEM numerical simulations are further validated by comparison of forces and wake inflow velocity with those measured experimentally at the U.S. Naval Academy. This is an important assessment, in that preliminary investigations have demonstrated that in IGE conditions the prediction of the wake shape in proximity of the ground significantly affects the evaluated rotor performance (especially the induced power, which is directly related to wake-induced velocity). This implies that, it is crucial to ensure the satisfaction of the impermeability boundary condition on the ground, to provide an accurate simulation of the wake shape and hence rotor loads. Since the satisfaction of the impermeability boundary condition on ground modeled through a distribution of sources and doublets is well-known to be a difficult numerical task[13], in this work the mirror image method which effectively enforces this type of boundary condition[18] is applied.

4. RESULTS

Given the geometry of the rotor tested at the U.S. Naval Academy facilities, the aerodynamic BEM solver is applied by using 2000 quadrilateral panels for each blade surface discretization, 200 panels for the discretization of the cylinder representing the motor surface, whereas the wake surface is discretized by 72000 panels. Figure 3 shows the implemented rotor/mirrored-rotor geometry, with the red plane representing the symmetry plane in the case of parallel ground.

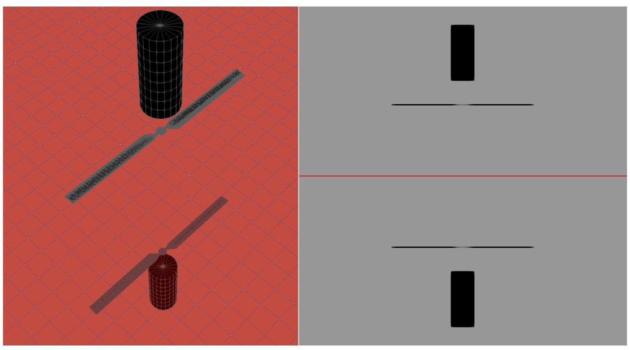

Figure 3: Rotor/mirrored-rotor configuration examined in the numerical simulation.

The flow field velocity to be compared with PIV data is evaluated over a rectangular grid of 120×90 control points placed on a plane perpendicular to the rotor disk, with a 180/rev sampling frequency, averaged over 50 rotor revolutions. Performance parameters are averaged over 50 rotor revolutions, as well. Both averages are evaluated after conclusion of a thirty-revolution transient.

4.1. Performance Analysis

Since the aerodynamic solver applied does not account for viscous effects, rotor performance is examined in terms of induced power coefficient, C_{P_i}. The figure of merit, FM, estimated through experimental data is used to relate the induced power with the total measured power coefficient, C_P, by the formula

$$FM = C_{P_i}/C_P$$

Then, for the rotor in IGE condition at the ground angle $\theta_g = 6°$, Fig. 4 shows the comparison of the experimental and numerical correlations between the normalized induced power coefficient (C_{P_i}/σ, with σ denoting the rotor solidity) and the normalized thrust coefficient, C_T/σ. An excellent agreement between predicted and measured power and thrust coefficient correlations is observed, although it is worth pointing out that, for a given trim condition, the blade collective pitch considered in the numerical solver is higher than that applied in the experiments.

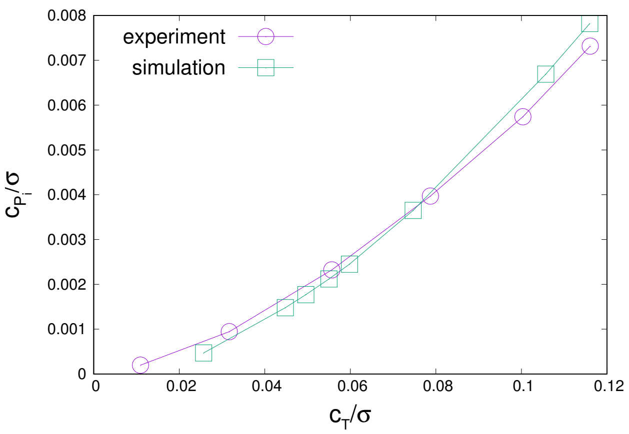

Figure 4: C_{P_i}/σ vs C_T/σ, for $\theta_g = 6°$.

Then, given a collective blade pitch angle θ_0, Fig. 5 shows the comparison between experimental and numerical correlations of C_{P_i}/σ and C_T/σ, for several values of the ground plane angle ($\theta_g = \{0°;\ 6°;\ 10°;\ 15°;\ 20°;\ 30°\}$). In this figure, experimental data for two fixed ground plane angles ($\theta_g = 0°$ and $\theta_g = 30°$) and different values of the rotor pitch angle are also highlighted. The general trends of predicted and measured coefficient correlations are in satisfactory agreement (when the ground angle increases the rotor performance decreases). It may be noted that the numerical results show a more regular (monotonic) behavior of the examined correlation than that shown by the experimental data. This could be due to the potential-flow assumption of the BEM formulation, as well as to a some uncertainties necessarily present in the measurements.

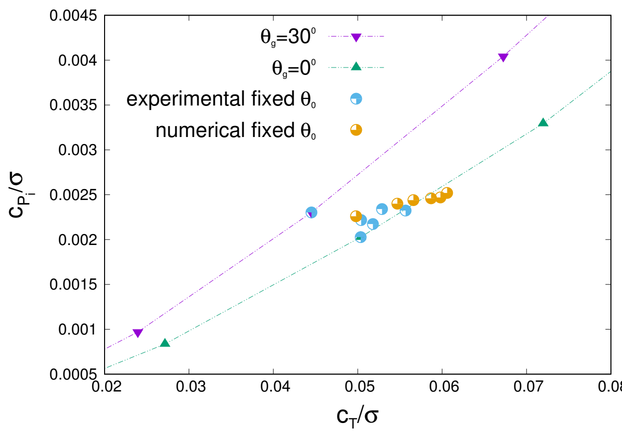

Figure 5: C_{P_i}/σ vs C_T/σ, for fixed pitch angle.

4.2. Flow Field

In the following, comparisons of measured and simulated flow fields are shown for $\theta_g = \{0°;\ 6°;\ 15°;\ 30°\}$. Velocity magnitude is presented as normalized by the analytic mean induced velocity, namely $v_h = \Omega R\sqrt{C_T/2}$.

Figure 6 shows the flow field evaluated numerically for the parallel-ground case ($\theta_g = 0°$). Comparing it with the corresponding experimental measurements depicted in Fig. 1, a good agreement is observed. As expected, in both figures the wake is nearly symmetric about the rotational axis. The main characteristics of the experimental flow field are well captured by the aerodynamic solver. The most relevant discrepancies between Figs. 6 and 1 are the slight numerical overestimation of the extension of the region affected by the tip vortices (namely, the larger extension of the outer red regions in Fig. 6), and the reduced numerical upstream velocity in the inner region (near the rotational axis).

Next, Fig. 7 depicts the numerical/experimental comparison of the flowfield for inclined ground with $\theta_g = 6°$. A good agreement between numerical and experimental data can be observed. Since the ground is not parallel to the rotor disk, the wake

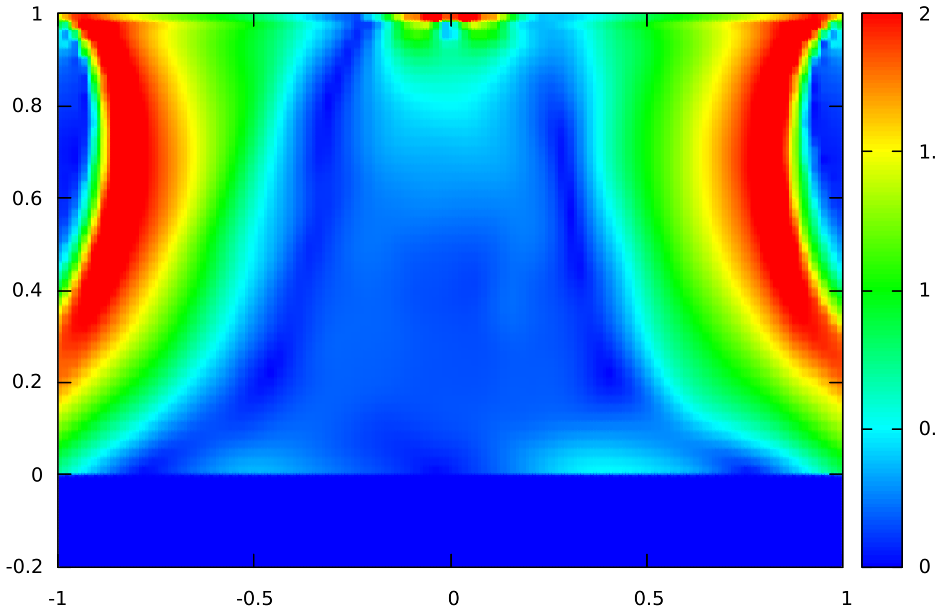

Figure 6: Numerical prediction of flow field with parallel ground.

and hence the flow field become asymmetric, with the uphill side of the wake forced to expand radially more rapidly than the downhill one. Also in this case the main difference between numerical and experimental flow field is in the inner region where the aerodynamic solver predicts lower velocities.

Figure 8 shows the same comparison for the ground plane angle $\theta_g = 15°$. Here, the loss of symmetry is more evident, and in the inner part of the wake a reduction of the stagnant flow region can be seen in both the numerical and the experimental data, with a slightly underestimation in the prediction of the velocity magnitude by the aerodynamic solver.

The flowfield occurring for the ground plane angle $\theta_g = 30°$ is presented in Fig. 9. A further reduction of the extension of the stagnant flow region in the inner part of the rotor wake and in proximity of the uphill side of the ground plane can be observed in both numerical and experimental data. In the proximity of the downhill side of the ground, instead, an increase of the magnitude of the jet-like flow is present.

A more detailed analysis of the wake structure is provided in Figs. 10, 11, 12 and 13 which present the comparison between experimental and numerical streamlines for the ground plane inclination angles considered in the previous figures.

For the parallel ground (Fig.10), the aerodynamic solver well captures the presence of the two large recirculation zones below the rotor. However, due the lower velocity in the inner part of the wake region, each of the recirculation zones in the numerical simulation is divided in two different structures.

Increasing the ground plane inclination angle, the wake becomes asymmetric and the formation of two wall-jet like flows appears, one convecting outboard, as in the parallel ground case, and one convecting inboard. For small ground angles (Figs. 11 and 12), the two recirculation zones below the rotor move towards the rotor hub, until they merge for $\theta_g = 30°$ when a unique large region of rotational flow can be seen around the hub (Fig. 13). This behavior is well captured by the numerical simulations, but due to the lower intensity of velocity magnitude predicted in the inner part of the wake, the streamlines in those recirculation zones are not perfectly predicted. Moreover, it is important to highlight that the aerodynamic solver well predicts the position of the stagnation point on the ground for all of the ground plane inclination angles examined. Therefore it is expected that the evaluation of loads on the ground (not available from experimental measurements) should be reasonably accurate.

Finally, in order to examine the effect of the ground plane inclination angle on the radial distri-

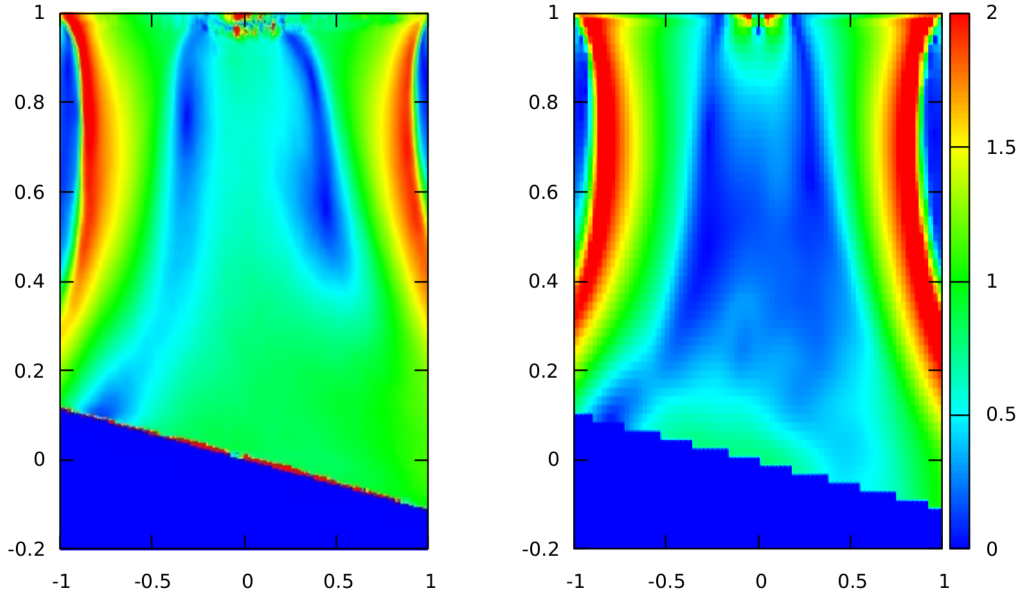

Figure 7: Flow field comparison for $\theta_g = 6°$; left side: experimental data; right side: numerical simulation.

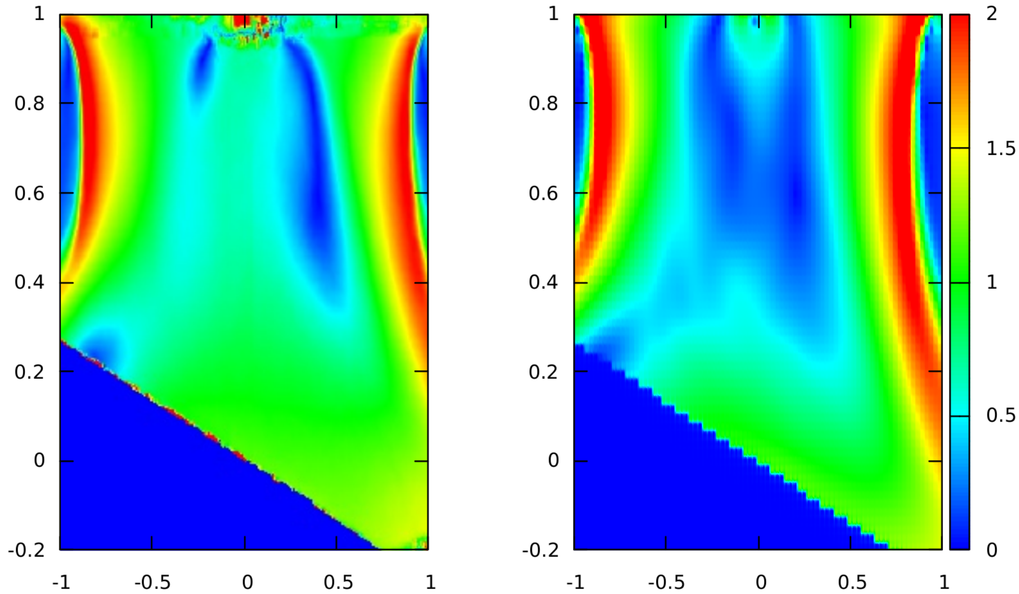

Figure 8: Flow field comparison for $\theta_g = 15°$; left side: experimental data; right side: numerical simulation.

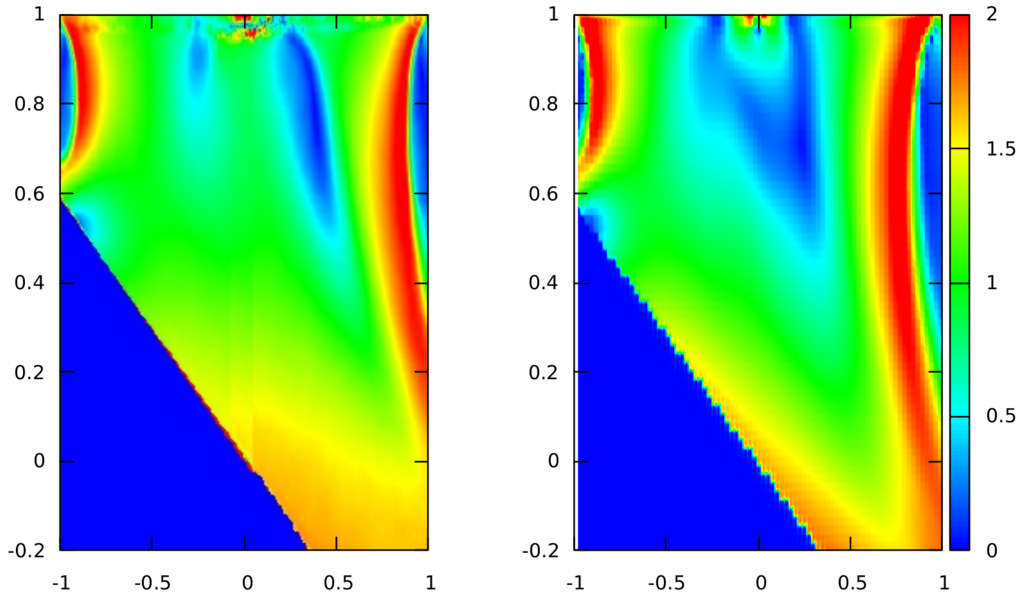

Figure 9: Flow field comparison for $\theta_g = 30^\circ$; left side: experimental data; right side: numerical simulation.

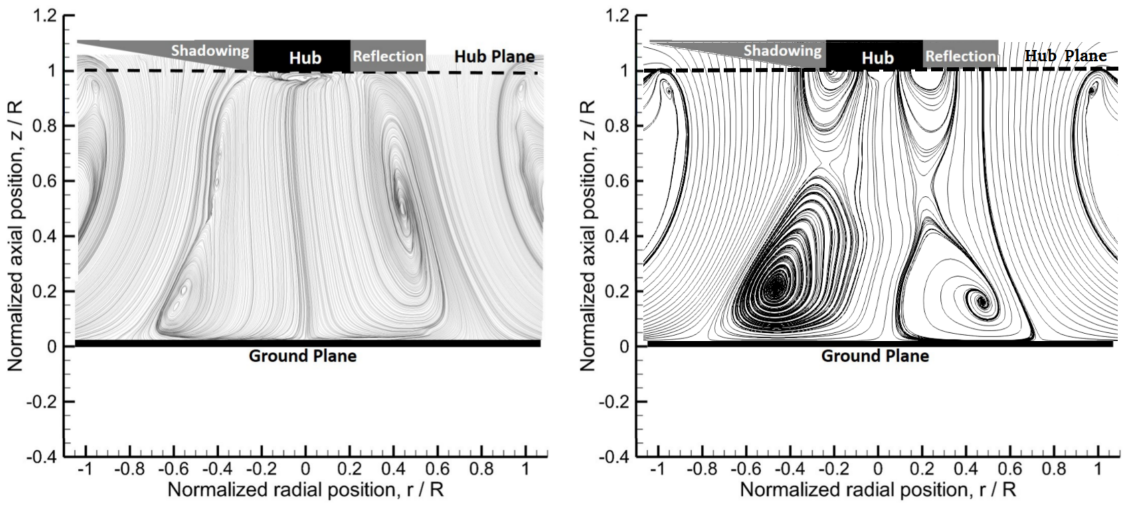

Figure 10: Comparison between experimental (left) and numerical (right) streamlines for $\theta_g = 0^\circ$.

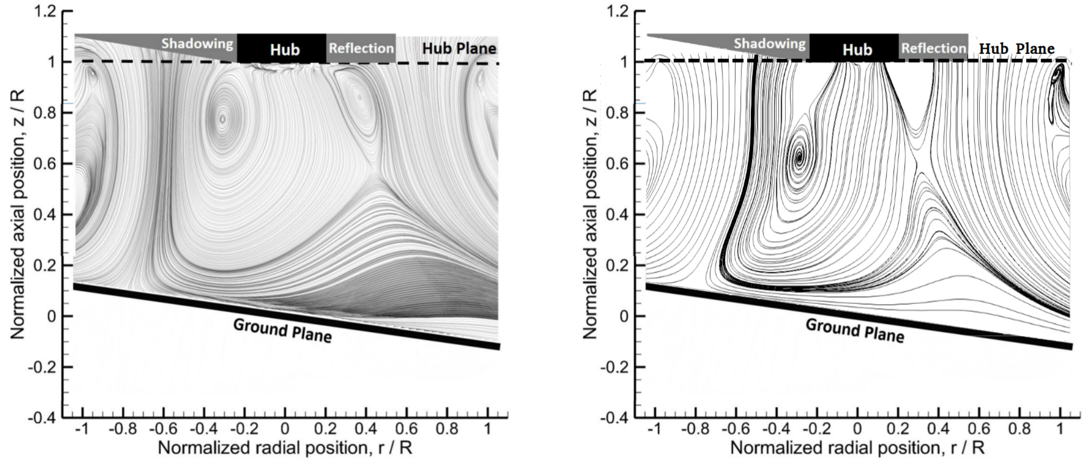

Figure 11: Comparison between experimental (left) and numerical (right) streamlines for $\theta_g = 6°$.

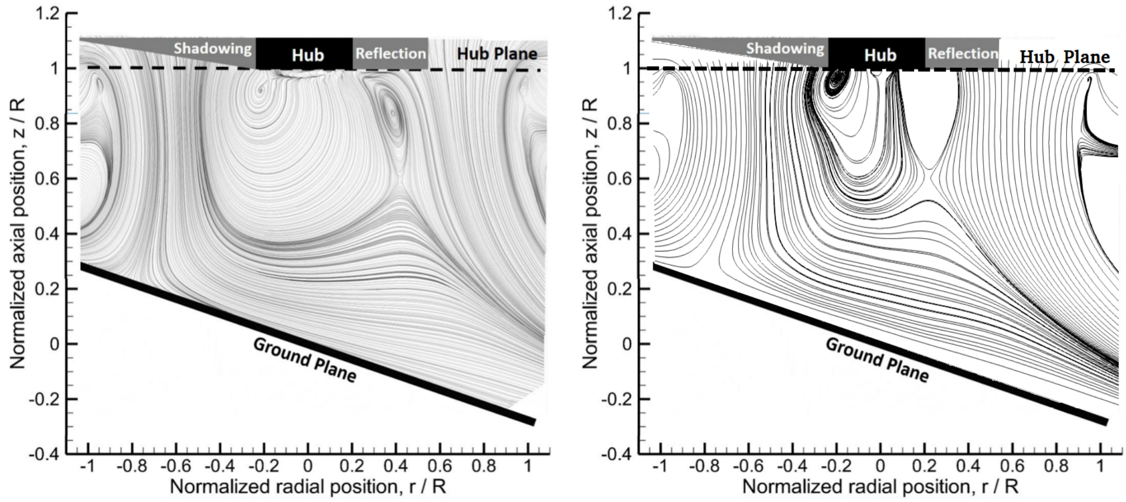

Figure 12: Comparison between experimental (left) and numerical (right) streamlines for $\theta_g = 15°$.

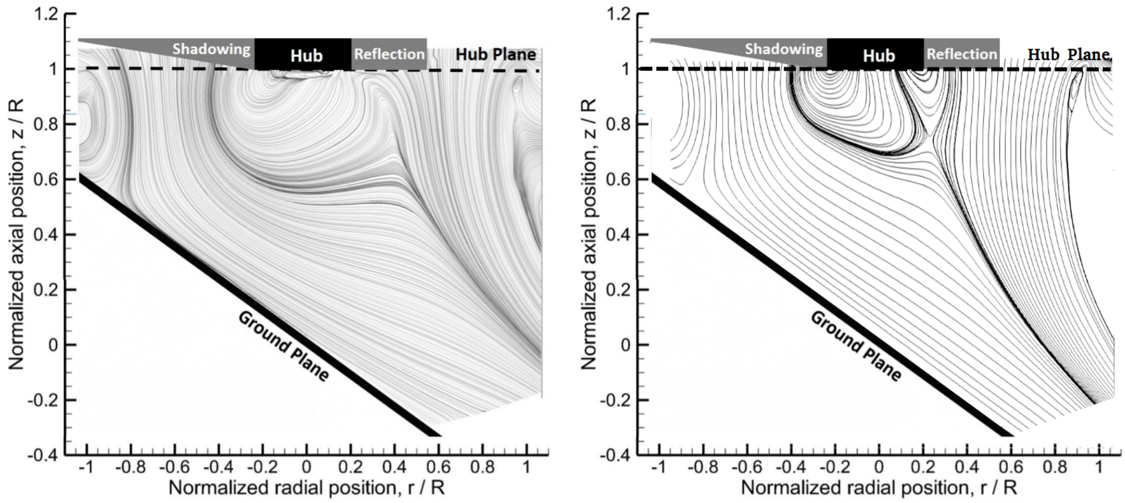

Figure 13: Comparison between experimental (left) and numerical (right) streamlines for $\theta_g = 30°$.

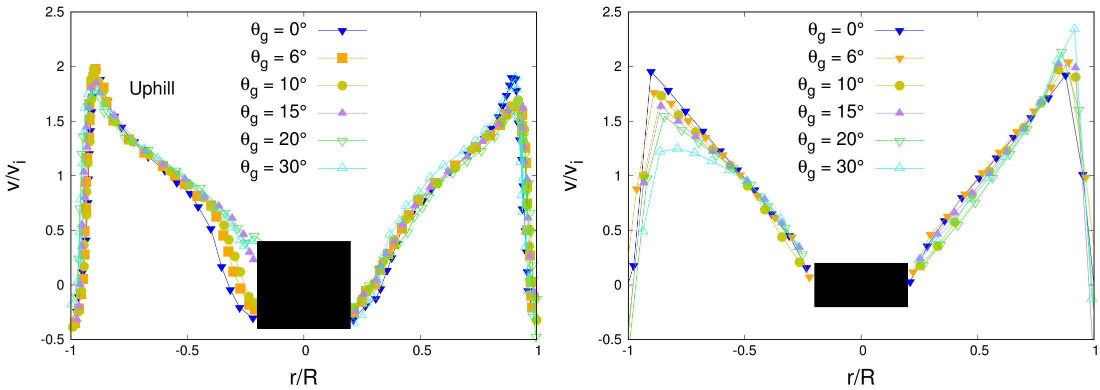

Figure 14: Comparison between experimental (left) and numerical (right) inflow axial velocity for several values of θ_g.

bution of wake inflow in proximity of the rotor disk, the normalized axial velocity over a line at $z/R = 0.99$ (just below the rotor disk) is plotted in Fig.14 for different ground plane inclination angles. In this case, some noticeable discrepancies between numerical and experimental data are observed. In particular, as the ground angle increases, numerical data show a clearly visible inflow velocity modification trend which is not present in the experimental data. Indeed, starting from the parallel ground case, in which the radial distribution is almost symmetric, as the ground angle increases, the numerical simulations show reduced axial velocity in the uphill side and increased axial velocity in the downhill side. This seems to be in agreement with the observed deformation of the wake and corresponding reduction of the inflow over the rotor as a parallel ground gets closer to the rotor (indeed, increasing the ground angle the uphill side gets closer to the blades).

5. CONCLUSIONS

Performance and flowfield of an in-ground-effect two-bladed helicopter rotor have been examined for several inclinations of the ground plane with respect to the rotor disk. Specifically, experimental data obtained by an experimental test campaign performed at the U.S. Naval Academy have been compared with the predictions of a BEM solver for potential flows, in order to assess its capability to provide high-fidelity simulations of IGE rotors aerodynamics. The test campaign included the examination of ground plane inclination angles ranging from 0° to 30° for a fixed collective blade pitch angle, as well as several rotor loading conditions for a given ground plane inclination angle. Numerical/experimental correlations have been made in terms of rotor induced power and thrust coefficients, but also in terms of flowfields and wake structures correlations, by comparing inflow velocity contour maps and streamlines over a plane perpendicular to the rotor disk. The following conclusions may be drawn:

- For the simulation of ground effect, the accurate satisfaction of the impermeability boundary condition over the ground is a crucial issue to capture the physics of the phenomenon with a suitable degree of accuracy. The mirror image method has confirmed to be more suited to enforce such a condition in a potential aerodynamic solver than the alternative approach based on the representation of the ground through a distribution of sources and doublets.

- IGE rotor performance is well predicted by the proposed aerodynamic solver, as demonstrated by numerical/experimental correlations involving rotor induced power coefficient and rotor thrust coefficient.

- Flowfield comparisons have demonstrated the capability of the aerodynamic solver to capture the wake deformation due to the presence of the ground with a good level of accuracy. Velocity contour maps show a good agreement between experimental data and numerical simulations. The mean features of the flowfield are well captured, except for the inner wake region where the velocity magnitude is underestimated.

- Streamlines visualization proves that the aerodynamic solver is able to capture the presence of the recirculation zones in the inner part of the wake, the stagnation region on the ground plane, as well as, the effect of ground plane inclination increase.

- The analysis of the radial distribution of the axial velocity induced on the rotor disk shows some discrepancies between experimental data and the simulations. In particular, the numerical evaluation of the velocity shows a variation of the distribution over the disk which is coherent with what is expected from the analysis of the velocity maps and the streamlines, namely, decreased upstream velocity and increased downstream velocity with the increase of the ground angle. This trend is not shown clearly by the experimental data. This fact, which deserves detailed additional study, could be due to phenomena related to the wake turbulent structures not modeled in the potential-flow simulation, as well as to some uncertainties inherently present in the measurement process.

ACKNOWLEDGEMENTS

This research was performed within the Roma Tre University participation in the University of Maryland/U.S.Naval Academy Vertical Lift Research Center of Excellence.

REFERENCES

[1] G. Bernardini, J. Serafini, S. Ianniello, and M. Gennaretti. Assessment of computational models for the effect of aeroelasticity on bvi noise prediction. *International Journal of Aeroacoustics*, 6(3):199–222, 2007.

[2] G. Bernardini, J. Serafini, M. Molica Colella, and M. Gennaretti. Analysis of a structural-aerodynamic fully-coupled formulation for aeroelastic response of rotorcraft. *Aerospace Science and Technology*, 29(1):175–184, 2013.

[3] H. Curtiss, M. Sun, W. Putman, and E. Hanker. Rotor aerodynamics in ground effect at low advance ratios. *Journal of the American Helicopter Society*, 29(1):48–55, 1984.

[4] M. Gennaretti, C. Bernardini, J. Serafini, and G. Romani. Assessment of a comprehensive aero-acousto-elastic solver for rotors in bvi conditions. In *43nd European Rotorcraft Forum*, 2017.

[5] M. Gennaretti and G. Bernardini. Novel boundary integral formulation for blade-vortex interaction aerodynamics of helicopter rotors. *AIAA Journal*, 45(6):1169–1176, 2007.

[6] M. Gennaretti, G. Bernardini, J. Serafini, and G. Romani. Rotorcraft comprehensive code assessment for blade-vortex interaction conditions. *Aerospace Science and Technology*, 80:232–246, 2018.

[7] M. Gennaretti, R. Gori, F. Cardito, J. Serafini, and G. Bernardini. A space-time accurate finite-state inflow model for aeroelastic applications. In *American Helicopter Society International 72nd Annual Forum*, 2016.

[8] M. Gennaretti, R. Gori, J. Serafini, F. Cardito, and G. Bernardini. Identification of rotor wake inflow finite-state models for flight dynamics simulations. *CEAS Aeronautical Journal*, 8(1):209–230, 2017.

[9] M. Gennaretti, L. Luceri, and L. Morino. A unified boundary integral methodology for aerodynamics and aeroacoustics of rotors. *Journal of Sound and Vibration*, 200(4):467–489, 1997.

[10] M. Gennaretti, C. Pasquali, F. Cardito, J. Serafini, G. Bernardini, and R. Celi. Dynamic wake inflow modeling in ground effect for flight dynamics applications. In *AHS 73nd Annual Forum & Technology Display*, 2017.

[11] D. A. Griffiths, S. Ananthan, and J. G. Leishman. Predictions of rotor performance in ground effect using a free-vortex wake model. *Journal of the American Helicopter Society*, 50(4):302–314, 2005.

[12] M. Knight and R. A. Hegner. Analysis of ground effect on the lifting airscrew. 1941.

[13] P. Ploumhans and G. Winckelmans. Vortex methods for high-resolution simulations of viscous flow past bluff bodies of general geometry. *Journal of Computational Physics*, 165(2):354–406, 2000.

[14] R. W. Prouty. Ground effect and the helicopter. In *AIAA/AHS/ASEE Aircraft Design System and Operations Meeting*, 1985.

[15] T. R. Quackenbush, D. B. Bliss, D. A. Wachspress, A. H. Boschitsch, and K. Chua. Computation of rotor aerodynamic loads in forward flight using a full-span free wake analysis. 1990.

[16] M. Ramasamy and J. G. Leishman. Interdependence of diffusion and straining of helicopter blade tip vortices. *Journal of Aircraft*, 41(5):1014–1024, 2004.

[17] M. Schmid. Simulation of helicopter aerodynamics in the vicinity of an obstacle using a free wake panel method. In *43rd European Rotorcraft Forum (ERF 2017)*, 2017.

[18] Y. Young and S. Kinnas. Analysis of supercavitating and surface-piercing propeller flows via bem. *Computational Mechanics*, 32(4-6):269–280, 2003.